Nanobiotechnol (2007) 3:197–202
DOI 10.1007/s12030-008-9013-1

Nano-Raman Spectroscopy: Surface Plasmon Emission, Field Gradients, and Fundamentally Near Field Propagation Effects

H. D. Hallen

Published online: 9 January 2009

Abstract Nano-Raman spectra differ from far-field Raman spectra. The differences result from a strong electric field gradient near the metal tip, propagation, and polarization, but the dependence upon probe-sample distance can only be explained by the inclusion of surface plasmons and the near-field, non-propagating terms of the dipole emission. A simple model based upon these components accurately describes distance-dependent data measured with a near-field scanning optical microscope. Our essentially near-field model will apply generally to Raman spectroscopy near a nanoscale conductor.

Keywords nano-Raman spectroscopy · near-field scanning optical microscopy · electric field gradients · surface plasmon emission · radially polarized Fresnel reflection

Plasmons are increasingly being recognized [1] for their role in optical interactions near nanoscale conductors. Most studies focus on the ability of plasmons to locally concentrate the electric field [2]. For Raman spectroscopy, this yields enhancements observed in surface-enhanced Raman spectroscopy [3–5]. We present here a different type of plasmon effect, one that modulates the efficiency of emission of Raman-shifted light with local geometry rather than simply providing more electric field for excitation. In particular, the plasmon absorbs the Raman-emitted light when momentum conservation allows the formation of the plasmon. Experimentally, this is observed as a dip in the Raman emission as the tip is retracted from the sample surface. The plasmon is generated on the metal that forms the aperture at the tip. The tip-sample distance dependence and the modes observed are influenced by several near-field factors described below. After these properties are described, then the experimental setup is summarized, and the insights from the properties are used to build a simple model that describes the plasmon effect. A slightly more complex model gives insights into other details of the tip-sample distance dependence.

Several factors influence nano-Raman spectroscopy. Most result directly or indirectly from the metal that is used to localize the light so that nanoscale resolution can be attained. Because of this, the same effects will be observed in Raman spectra *of all constituents* of complex nanostructured materials that contain a metallic component. The near-field scanning optical microscope (NSOM) provides a useful tool for understanding these effects, since it can be moved with respect to the molecules under study, providing measurements that the modeling must describe. The metal quenches any electric field near a conducting surface that is not polarized perpendicular to the surface. This forces a strong gradient in the electric field component perpendicular to the metal surface in light propagation near a small metal object, since propagating light must be transverse away from the metal. The transition from normal to transverse polarization occurs in a scale of tens of nanometers, resulting in a very strong field gradient. This gradient allows a coupling between the optical field and a vibration known as gradient-field Raman (GFR) spectroscopy [6, 7] and provides the dominant contribution to the observed functional dependence of spectral peak amplitude versus probe sample distance. This coupling acts in addition to the normal Raman coupling but has different selection rules, which favor bonds perpendicular to the metal surface with strong infrared coupling and largely complement normal Raman.

H. D. Hallen (✉)
Department of Physics, North Carolina State University Raleigh, Raleigh, NC 27695-8202, USA
e-mail: Hans_Hallen@ncsu.edu

The second property impacting the observed spectra results from propagation considerations. Light underneath an NSOM probe such as that shown in Fig. 1a must propagate around the probe end before it can be collected in reflection [8]. Light polarized normal to the surface can propagate easily, whereas transverse polarized light tends to propagate downwards, where it contributes instead to transmitted light. Thus, spectroscopy in reflection limits collected light to vibration modes that emit with electric field normal to the surface, such as those with GFR coupling. Other special geometries can also markedly effect collection [9, 10]. In this work, the Raman spectra are collected in reflection.

The spatial polarization distribution of light emanating from a small aperture, the 3rd property, has been calculated [11, 12] and measured with NSOM of simple molecules [13]. We use this as an illumination source in our model. Figure 1c, d show plots of the magnitude of the x- (input) and z- (normal) components of electric field (E) squared at a distance of 0.1 apertures beyond the probe end. All components of E are present with an x-polarized source, since they are required to satisfy the boundary conditions [14]. The z- or normal component is large just outside the aperture, as expected from Fig. 1c. The integrated intensity shows the strong lightning-rod-like enhancement of the electric field under the probe. We do not consider plasmon-enhanced illumination fields, which would have similar qualitative properties.

When a metal is near an oscillating dipole, it affects the emission of light, the fourth property. This has been observed in fluorescence lifetime measurements with NSOM [15, 16]. The lifetime is altered by the presence of the metal [17–20]. At longer distances, plasmons become important, but only if momentum conservation can be

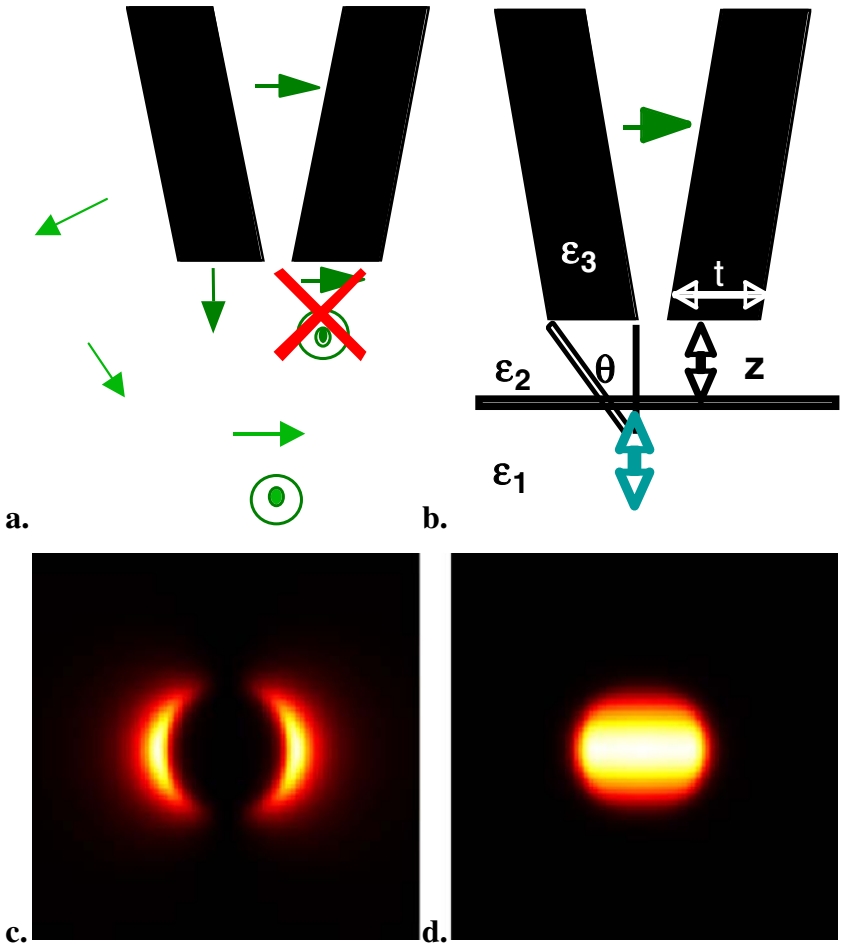

Fig. 1 **a** A schematic drawing of an NSOM probe tip, illustrating a typical metal thickness (*black*) surrounding the tip of the etched silica fiber. *Arrows* indicate the polarization of light at various points. The '*X*' emphasizes the boundary condition for electric field at a metal surface. **b** A schematic of the model geometry defines the dielectric constants, z-coordinate, and angle from the dipole emitting Raman-shifted light, *double arrow*, to the outer edge of the tip, where interacts with the metal and scatters to the detector. **c**,**d** Images of the calculated squared electric field components for x-polarized light input into the probe. The sizes of the images are three apertures in both x and y, centered a distance 0.1 apertures below the tip of the probe. **c** The z-component, with range 0.07 a.u, **d** The x-component, with range 0.16 a.u.

satisfied. When the surfaces are smooth, momentum conservation for plasmon generation typically requires that the light be incident from a substance with an index greater than that in which the surface plasmon propagates. In plasmon sensors [21], light incident through the substrate couples through the thin metal film to the free surface of the metal, where the surface plasmon propagates. In our system, the molecule (bond) resides in the substrate separated by a few nanometer thick air gap from the metal tip upon which the surface plasmons propagate. Momentum conservation is carried over the small distance by evanescent light. This is quite similar to the Otto configuration for surface plasmon studies [22] and differs from the widely used plasmon sensor configuration in which the metal resides on the material through which the light is incident. At few nanometer dipole to metal separations, such as when we stab the probe into the surface, the creation of electron–hole pairs, etc. in the metal become important, and the emission drops to zero [17].

The final ingredient, property 5, needed to accurately model the near-field Raman signal relate to the origin of the plasmon interactions, which result from inelastic reflections from the metal interfaces but arise mathematically from the interference of a wave reflected from the metal surface that supports the plasmon propagation with another wave that does not reflect from that surface. Our case differs from the typical case in three ways. First, the light propagates around the probe tip after the interaction, rather than reflecting into the material from which it came; second, the plane wave picture is only approximately valid since the region of interest is sub-wavelength in size; and third, most importantly, the dominant emission from the dipole in the near field is the non-propagating $'1/r^3'$ terms of the dipole radiation. We find that it is necessary to use these inherently near-field terms to model the behavior of the Raman signal. In particular, the radial-polarized term required has different reflection characteristics than either of the two polarizations found in the far field: parallel or perpendicular to the plane of incidence of the wave.

The nano-Raman spectra were collected as previously described [23]. Aluminum-coated-etched [24] fiber tips were positioned near the surface of samples under investigation, and spectra were taken with the tip near the surface under lateral force feedback [25–27]. The NSOM [28] was used in the illumination mode with 514 nm laser light. Reflected light is collimated with a 0.50 NA lens, passed through a holographic filter, focused into a single stage 1 m spectrometer, and collected with a cooled (–45°C) CCD camera. The sample is crystalline $KTiOPO_4$ (KTP).

Our model describes only the primary contribution to the Raman spectra so that the essential physics is clear. For collection in reflection, the dipole that emits the Raman-shifted light is, by property 2, optimally oriented with its axis normal to the surface, so its produces light with normal polarization. This is driven most efficiently by incident electric field normal to the surface, in the region of maximal field just outside the aperture (Fig. 1c (i.e., property 3)). This is the location we assume for the Raman interaction, and is indicated in Fig. 1b, which also defines several parameters in the equations below. The Raman-like signal available to propagate around the probe end is given by the interference between light reflected off the metal surface and the non-reflected wave that has also propagated across the $\varepsilon_1 -> \varepsilon_2$ interface. For plane waves approaching an interface, this is a standard result [19] and yields a plasmon resonance (in reflection) as a function of incident angle. Two factors render this inappropriate here: the dipole radiates in all directions since the illuminated region is subwavelength, and the dipole is so close to the surface the radiative (proportional to $1/r$, with r the dipole to observation point distance) terms of the electric field are small compared to the evanescent, near-field $1/r^3$ terms. The interaction is, thus, dominated by the "$1/r^3$" terms, property 5, that scatter from the NSOM probe tip corner to become propagating and form the reflection nano-Raman signal. There are two terms proportional to "$1/r^3$" resulting from dipole p_0 emission [29], one with radial polarization: $E_r = \left(2p_0/r^3\right)\cos(\theta)e^{-i(\omega t - kr)}$ and the other with transverse polarization $E_\theta = \left(2p_0/r^3\right)\sin(\theta)e^{-i(\omega t - kr)}$. For the angles θ required to reflect from the probe metal, it is the radial-polarized E_r term that is of interest here.

The Fresnel formulae permit calculation of the portion of light transmitted or reflected from the interface. Since E_r is polarized in the direction of propagation, its amplitude reflection coefficient E_r''/E_r is not given by the standard formula. Nevertheless, a formula follows from the same considerations as the usual formulae, from the boundary conditions of Maxwell's equations [30]. The derivation follows the standard one, starting with continuity of E parallel to the interface and εE perpendicular to the interface. The former implies $E_r''\sin\theta + E_r\sin\theta = E_r'\sin\theta'$ or $E_r'' + E_r = E_r'\sqrt{\varepsilon/\varepsilon'}$ using Snell's Law and θ the incident angle relative to normal, where the double prime refers to the reflected light and the single prime to transmitted light. The latter yields $-\varepsilon E_r''\cos\theta + \varepsilon E_r\cos\theta = \varepsilon' E_r'\cos\theta'$ or $\sqrt{\varepsilon}E_r''q + \sqrt{\varepsilon}E_r q = \sqrt{\varepsilon'}E_r'q'$ with $q_i = \frac{2\pi}{\lambda}\sqrt{\varepsilon_i}\cos\theta_i = \frac{2\pi}{\lambda}\sqrt{\varepsilon_i - \varepsilon_1\sin^2\theta_1}$. Combining these results we obtain

$$E_r''/E_r = (\varepsilon_2 q_2 - \varepsilon_3 q_3)/(\varepsilon_2 q_2 + \varepsilon_3 q_3) \quad (1)$$

for reflection from media 3 (with prime) while incident from media 2. We do not need the transmission coefficient from media 1 to 2, since both interfering waves cross it—it will be absorbed into a scale factor to be determined by the data. An exponential decay proportional to $exp(-\mathrm{imag}(q_2)z)$ affects both waves as the tip moves away from the sample is

included, since we need to calculate the tip-sample (z) distance dependence of the Raman signal. The quantity q_2 becomes imaginary as the incident angle increases beyond the critical angle for total internal reflection. Such large angles of incidence are required for momentum conservation as the light couples to the plasmon. The calculation uses the angle θ of the line that connects the point of the sample below the edge of the aperture to the edge of the probe, as shown in Fig. 1b. This angle is also dependent upon the tip-sample (z) distance. The line connects the region with strongest illumination of z-polarized light to the point where emitted light can scatter and be collected in reflection. The scattering point is not unique, as any point below the aperture ring can be connected to any point at the edge of the probe. We have tried averaging over all these points. Such an average introduces another parameter, the aperture size, but does not significantly affect the fit. Thus, we show results for only the θ shown in Fig. 1b, which depends upon the thickness t of the aperture metal and the distance z to the surface, $\tan\theta = t/z$. The Bethe-Boukamp [11, 12] model is used to calculate within a multiplicative constant the z-dependent gradient-field Raman signal, proportional to $\mathrm{BB} = E_z(dE_z/dz)$, by integrating over images such as that shown in Fig. 1c, d, as described in [6]. The field E_z is given in terms of the coordinates $v = \mathrm{sqrt}\left((\mathrm{sqrt}(b^2 + 4z^2) - b)/2\right)$, $u = z/v$ with $b = 1 - (\mathrm{x}^2 + \mathrm{y}^2 + \mathrm{z}^2)$ as $E_z = 8axv/((u^2 + v^2)(1 + v^2))$. We scale this z-dependent result by the z-dependent exponential decay $\exp(-\mathrm{imag}(q_2)z)$ and interfere (add then take the magnitude) the reflected and non-reflected waves, which differ by the z-dependent (through θ) complex factor given in Eq. 1:

$$\mathrm{Raman}_{\mathrm{Model}} = C\left|(\varepsilon_2 q_2 - \varepsilon_3 q_3)/(\varepsilon_2 q_2 + \varepsilon_3 q_3) + 1\right| \times \exp(\mathrm{imag}(q_2)z)\cos\theta \int\int \mathrm{BB}\,\mathrm{dxdy} \quad (2)$$

where C is a scaling constant, as noted above.

The result is shown in Fig. 2, where the model (Eq. 2) with and without the plasmon (Eq. 1) term is compared to the experimental 787 wavenumber peak in KTP [6]. The curve drops smoothly with distance except for a sharp minimum within which the value drops close to zero. The narrow minimum is the effect of the plasmon absorbing the energy emitted by the dipole. The result depends upon two parameters, the thickness of the metal coating of the aperture, which we know approximately, and an overall scaling factor for the result. The primary influence of a different thickness t is to move the z-value of the narrow dip. Thus, the shape of the curve is not influenced by either

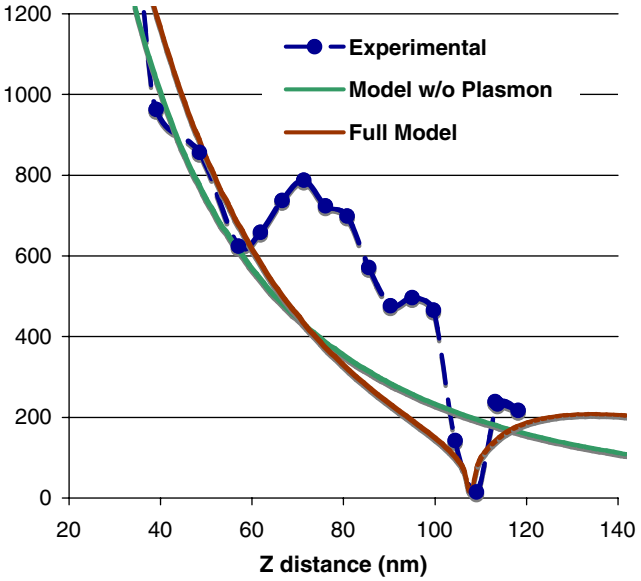

Fig. 2 The measured nano-Raman signal, *dots with dotted line*, is compared to a model that incorporates field gradient effects but not plasmons, and the same model augmented to include plasmon generation. Both models have an arbitrary scale factor applied.

of the parameters. The similarity to the measured data is remarkable given the simplicity of the model and the few adjustable parameters. We attempted to fit the observed minima in Fig. 2 with non-radial polarized Fresnel reflected light without even qualitative success, indicating the qualitative difference between the near-field and far-field light, and reinforcing property 5, that the radial-polarized $1/r^3$ fields dominate near-field Raman emission.

Although the minimum in the measured data is accurately modelled by the simple model as a plasmon effect during the Raman emission process, the bump to the left of the minimum is not apparent at all in the model. We investigate a slightly more complex model to gain some insight into the origins of that feature. The simple model that includes plasmons will now be termed the single bounce model. Another model will be created as shown in Fig. 3a that has two bounces. It will use the same insights to position the Raman emitter where the z-polarized excitation light is greatest, so that the signal will be optimally transmitted to the far-field detection behind the probe. The radially polarized equations will also be used. The only difference is that the ray with two bounces undergoes an additional reflection and has a different phase due to the longer propagation distance. In particular, the term in the brackets in Eq. 2 is changed:

$\left|(\varepsilon_2 q_2 - \varepsilon_3 q_3)/(\varepsilon_2 q_2 + \varepsilon_3 q_3) + 1\right|$ becomes
$$\left|(\varepsilon_2 q_2 - \varepsilon_3 q_3)/(\varepsilon_2 q_2 + \varepsilon_3 q_3) \times (\varepsilon_2 q_2 - \varepsilon_1 q_1)/(\varepsilon_2 q_2 + \varepsilon_1 q_1) \times \exp\left(-i\,2.3 \times 2\pi z\sqrt{\varepsilon_2/\lambda}\right) + 1\right|, \quad (3)$$

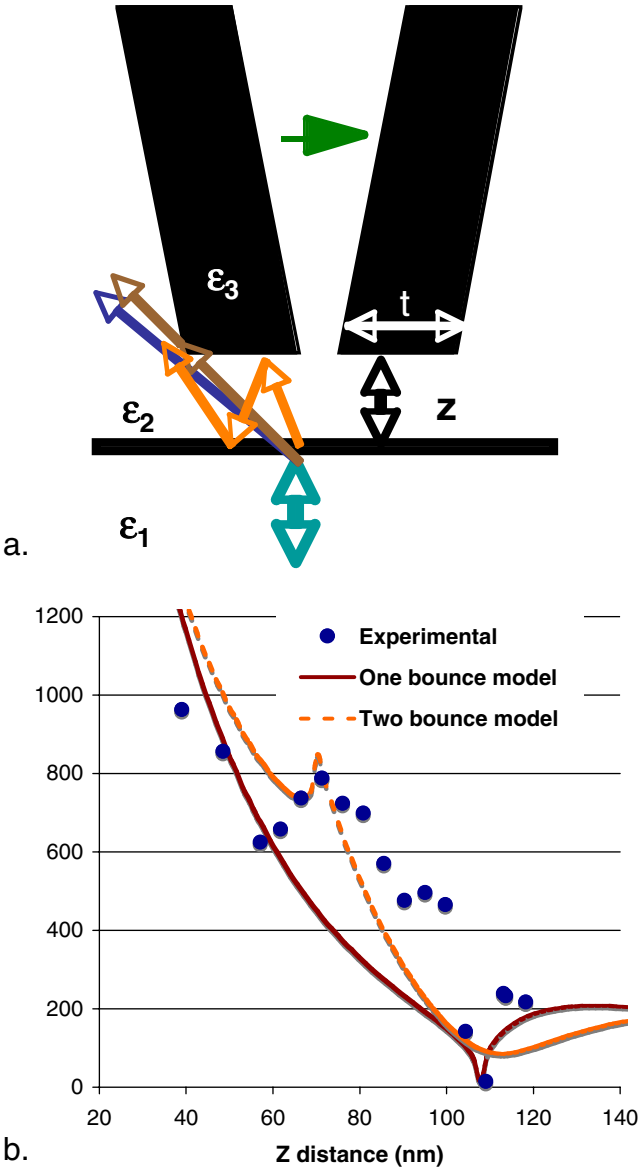

Fig. 3 Two models for the nano-Raman signal are considered. **a** A schematic drawing shows the single bounce case and the two-bounce case. The former yields a model with one less parameter than the second. **b** The measured nano-Raman signal, *dots*, is compared to the two models. Both incorporate field gradient effects, include plasmon generation and near-field radial-polarization reflection coefficients, and have an arbitrary scale factor applied. The difference is a second reflection and more path length for the two-bounce case.

where the 2-bounce ray has the reflection off layer 3 from layer 2, the reflection off layer 1 from layer 2, and the phase change associated with propagating $2.3 \times z$ in media 2. All other factors are taken to be the same, so the ray without reflection is represented by the 1. The reader may note that the angles are different for the rays, and the phase factor not exact (and invariant with the angle θ, which changes as z changes). We simplified these aspects of the model since they add additional complication without providing a significant change in the curve. Further, as noted above, the use of rays, or plane waves, in the description of such a process in a sub-wavelength region is not fully justified, although it has been shown to remain a reasonable approximation beyond what would naively be considered to be the case [31]. Nevertheless, to provide an exact calculation with a fundamentally defective model would not be prudent, so we do not. We find that the two-bounce model does have both the bump and the minima as the *z*-distance is increased, although the bump is to narrow and the minima too broad. This is not as much of a problem as it may appear, however, since we have calculated the two-bounce model for only one direction of emission. It will, in general, emit around the entire radius of the probe tip. Other scattering points on the aperture radius will have larger θ-values for a give *z*-value, which means that the features will occur (same θ-value) at larger *z*-distances. In other words, averaging the signal will spread the bump and cancel some of the width of the minimum. We do not show those results since the model is not accurate enough, due to the above-mentioned problems, to warrant the additional parameter (aperture size) that would be required.

Spectroscopy of any constituent in a complex, metal containing, material must be considered for the properties described here: (1) field gradients, (2) propagation, (3) illumination field in the region of interest, (4) surface plasmons and other loss to the metal, and (5) dominance of the non-propagating fields. New spectroscopic features or a change in relative intensities can result from property 1. Loss of expected features can be caused by properties 2 or 4. The detection of molecules will be position-dependent due to property 4. All effects depend upon the distance to the metal surface. Quantification can be hindered because the signal amplitude depends on the location of a component in addition to the quantity of that component present. Between properties 1 and 3, we note that it is possible to identify all 3 dimensions of Raman vibration modes and IR-like vibrations normal to the surface with nanometer-scale resolution using apertured NSOM-Raman.

In summary, we have shown that surface plasmons can influence the emission of near-field Raman scattered light. A very simple model gives a good description of the tip-sample separation dependence of Raman lines in near-field Raman, and illustrates the true near-field nature of the process.

Acknowledgement This material is based upon work supported by the National Science Foundation under Grant Nos. DMR-9975543 and DMII-0210058. We acknowledge technical discussions with Catherine Jahncke and Eric Ayars.

References

1. Mansuripur M, Li L. What in the world are surface plasmons. Optics Photonics News. 1997;8:50–5. May.
2. Milner RG, Richards D. The role of tip plasmons in near-field Raman microscopy. J Microscopy. 2001;202(Pt 1):66–71.
3. Moody RL, Vo-Dinh T, Fletcher WH. Investigation of experimental parameters for surface-enhanced Raman scattering (SERS) using silver-coated microsphere substrates. Appl Spectrosc. 1987;41 (6):966–70.
4. Baker GA, Moore DS. Source, "Progress in plasmonic engineering of surface-enhanced Raman-scattering substrates toward ultra-trace analysis". Anal Bioanal. Chem 2005;382(8):1751–70.
5. Xu H, Wang X-H, Persson MP, Xu HQ, Kall M, Johansson P. Unified treatment of fluorescence and Raman scattering processes near metal surfaces. Phys Rev Lett. 2004;93(24):243002–1–4.
6. Ayars E, Hallen HD, Jahncke CL. Electric field gradient effects in Raman spectroscopy. Phys Rev Lett. 2000;85(19):4180–3.
7. Hallen HD, Jahncke CL. The electric field at the apex of a near-field probe: implications for nanoRaman spectroscopy. J Raman Spectroscopy. 2003;34(9):655–62.
8. Jahncke CL, Ayars EJ, Hallen HD. The effects of probe boundary conditions and propagation on nano-Raman spectroscopy. J Microsc. 2003;210(Pt 3):252–4.
9. Jackson JB, Westcott SL, Hirsch LR, West JL, Halas NJ. Controlling the surface enhanced Raman effect via the nanoshell geometry. Appl Phys Lett. 2003;82(2):257–9.
10. Poitras CA, Lipson M, Du H, Hahn MA, Krauss TD. Photo-luminesce enhancement of colloidal quantum dots embedded in a monolithic cavity. Appl Phys Lett. 2003;82(23):4032–4.
11. Bethe HA. Theory of diffraction by small holes. Phys Rev. 1944;66:163–82.
12. Bouwkamp CJ. On Bethe's theory of diffraction by small holes. Philips Res Rep. 1950;5:321.
13. Betzig E, Chichester RJ. Single molecules observed by near-field scanning optical microscopy. Science 1993;262:1422–5.
14. McDaniel EB, McClain SC, Hsu JWP. Nanometer scale polarimetry studies using a near-field scanning optical microscope. Appl Opt. 1998;37:84–92.
15. Ambrose WP, Goodwin PM, Martin JC, Keller RA. Alterations of single molecule fluorescence lifetimes in near-field optical microscopy. Science 1994;265:364–7.
16. Bian RX, Dunn RC, Xie XS, Leung PT. Single molecule emission characteristics in near-field microscopy. Phys Rev Lett. 1995;75 (26):4772–5.
17. Ford GW, Weber WH. Electromagnetic interactions of molecules with metal surfaces. Phys Reports. 1984;113(4):195–287.
18. Hellen EH, Axelrod D. Fluorescence emission at dielectric and metal-film interfaces. J Opt Soc Am B. 1987;4(3):337–50.
19. Lukosz W, Kunz RE. Light emission by magnetic and electric dipoles close to plane interface I Total radiated power. J Opt Soc Am. 1977;67(12):1607.
20. Weber WH, Eagan CF. Energy transfer from en excited dye molecule to the surface plasmon in an adjacent metal. Opt Lett. 1979;4(8):236–8.
21. Homola J, Yee SS, Gauglitz G. Surface plasmon resonance sensors: review. Sens Actuators, B. 1999;54:3–15.
22. Otto A. Z Phys. 1968;216:398.
23. Ayars E, Hallen HD. Surface enhancement in near-field Raman spectroscopy. Appl Phys Lett. 2000;76(26):3911–3.
24. Hoffmann P, Dutoit B, Salathé R-P. Comparison of mechanically drawn and protection layer chemically etched optical fiber tips. Ultramicroscopy 1995;61:165–70.
25. Betzig E, Finn PL, Weiner JS. Combined shear force and near-field scanning optical microscopy. Appl Phys Lett. 1992;60: 2484–6.
26. Toledo-Crow R, Yang PC, Chen Y, Vaez-Iravani M. Near-field differential scanning optical microscope with atomic force regulation. Appl Phys Lett. 1992;60:2957.
27. Karrai K, Grober RD. Piezoelectric tip-sample distance control for near-field optical microscopes. Appl Phys Lett. 1995;66:1842.
28. Jahncke CL, Hallen HD. A versatile, stable scanning proximal probe microscope. Rev Scient Instr. 1997;68:1759.
29. Heald M, Marion J. Classical electromagnetic radiation. 3rd ed. Pacific Grove: Brooks/Cole; 1995.
30. Guenther RD. Modern optics. New York: Wiley; 1990.
31. Yakobson BI, Paesler MA. Tip optics for illumination NSOM: extended zone approach. Ultramicroscopy 1995;57:204.